Characteristics and Crystal Structure of Bacterial Inosine-5′-monophosphate Dehydrogenase[†,‡]

Rong-guang Zhang, Gwyndaf Evans, Frank J. Rotella, Edwin M. Westbrook, Don Beno, Eliezer Huberman, Andrzej Joachimiak, and Frank R. Collart*

Center for Mechanistic Biology and Biotechnology, Argonne National Laboratory, 9700 South Cass Avenue, Argonne, Illinois 60439-4833

Received December 3, 1998; Revised Manuscript Received January 28, 1999

ABSTRACT: IMP dehydrogenase (IMPDH) is an essential enzyme that catalyzes the first step unique to GTP synthesis. To provide a basis for the evaluation of IMPDH inhibitors as antimicrobial agents, we have expressed and characterized IMPDH from the pathogenic bacterium *Streptococcus pyogenes*. Our results show that the biochemical and kinetic characteristics of *S. pyogenes* IMPDH are similar to other bacterial IMPDH enzymes. However, the lack of sensitivity to mycophenolic acid and the K_m for NAD (1180 μM) exemplify some of the differences between the bacterial and mammalian IMPDH enzymes, making it an attractive target for antimicrobial agents. To evaluate the basis for these differences, we determined the crystal structure of the bacterial enzyme at 1.9 Å with substrate bound in the catalytic site. The structure was determined using selenomethionine-substituted protein and multiwavelength anomalous (MAD) analysis of data obtained with synchrotron radiation from the undulator beamline (19ID) of the Structural Biology Center at Argonne's Advanced Photon Source. *S. pyogenes* IMPDH is a tetramer with its four subunits related by a crystallographic 4-fold axis. The protein is composed of two domains: a TIM barrel domain that embodies the catalytic framework and a cystathione β-synthase (CBS) dimer domain of so far unknown function. Using information provided by sequence alignments and the crystal structure, we prepared several site-specific mutants to examine the role of various active site regions in catalysis. These variants implicate the active site flap as an essential catalytic element and indicate there are significant differences in the catalytic environment of bacterial and mammalian IMPDH enzymes. Comparison of the structure of bacterial IMPDH with the known partial structures from eukaryotic organisms will provide an explanation of their distinct properties and contribute to the design of specific bacterial IMPDH inhibitors.

Inosine monophosphate dehydrogenase (IMPDH; EC 1.1.1.205)[1] is a rate-limiting enzyme in the synthesis of guanine ribonucleotides. IMPDH has an essential role in providing critical precursors for DNA and RNA biosynthesis and in signal transduction pathways that mediate cell differentiation (*1*, *2*). This essential nature is illustrated by the utility of IMPDH inhibitors as therapeutic agents. Several potent inhibitors of mammalian IMPDH enzymes are used clinically as antiviral, anticancer, or immunosuppressive agents (*3*−*5*). However, the utility of IMPDH inhibitors as antimicrobial agents has not been fully investigated.

Sequence analysis of all known IMPDH enzymes supports a distinction between the bacterial and eukaryotic enzymes. A deep branching of the bacterial and eukaryotic forms of IMPDH is observed upon phylogenetic analysis of the relationships among the various IMPDH genes (*6*, *7*). The analysis indicates a general functional conservation of amino acid residues and suggests a unique amino acid sequence signature for these kingdoms. The phylogenetic differences between IMPDH enzymes reflect their kinetic differences and differential sensitivity to inhibitors. Enzymes from mammalian sources show distinctly lower values for the K_m for NAD than do those enzymes from bacteria (*8*−*10*). In addition, mammalian IMPDH enzymes are several orders of magnitude more sensitive to inhibition by mycophenolic acid (MPA) than are bacterial IMPDH enzymes (*8*−*10*). We hypothesize that the biochemical and kinetic differences between bacterial and mammalian enzymes are a consequence of the variance of specific, identifiable amino acid residues. Identification of the critical residues or combination of residues is a prerequisite for the rational identification of agents that specifically target the bacterial enzyme.

IMPDH catalyzes the NAD-dependent oxidation of IMP to XMP, a primary step in the biosynthesis of guanine ribonucleotides. The reaction mechanism has been examined in detail for IMPDH from *Escherichia coli* (*11*), *Tritrichomonas foetus* (*12*), and humans (*13*). These enzymes use a sequential, ordered, bi-bi kinetic mechanism in which IMP binds before NAD and NADH is released before XMP

[†] This work was supported by the U.S. Department of Energy, Office of Biological and Environmental Research, under Contract W-31-109-ENG-38.

[‡] Coordinates and structure factors have been deposited in the Brookhaven Protein Data Bank (PDB) under ID code 1ZFJ.

* Correspondence should be addressed to this author. E-mail: Fcollart@anl.gov. Phone: 630-252-4859. Fax: 630-252-3387.

[1] Abbreviations: IMPDH, IMP dehydrogenase; GTP, guanosine triphosphate; IMP, inosine monophosphate; XMP, xanthosine monophosphate; MALDI-MS, matrix-assisted laser desorption ionization mass spectroscopy; MAD, multiwavelength anomalous diffraction; MPA, mycophenolic acid; PDB, Protein Data Bank; AU, asymmetric unit; NAD, nicotinamide adenine dinucleotide; MW, molecular weight; SeMet, selenomethionine; CBS, cystathionine β-synthase; FOM, figure of merit; IPTG, isopropylthiogalactopyranoside.

10.1021/bi982858v CCC: $18.00
Published on Web 03/26/1999

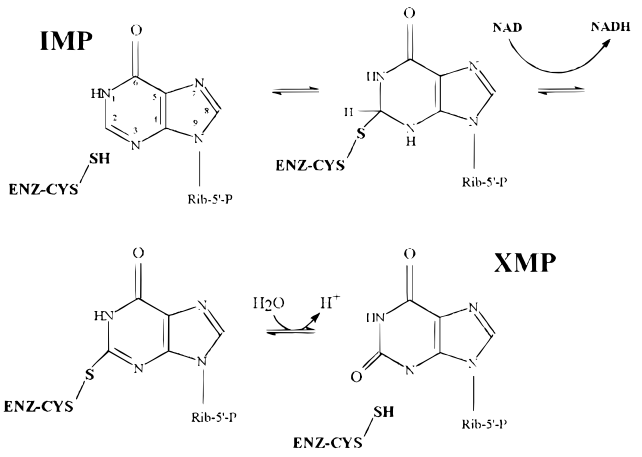

FIGURE 1: Reaction catalyzed by IMPDH.

(Figure 1). The reaction proceeds through a covalent linkage between C2 of IMP and the sulfhydryl of an active site cysteine (Cys310 in *S. pyogenes)*. A hydride transfer to NAD is thought to occur from this intermediate followed by hydrolysis of the oxidized enzyme−IMP complex to yield XMP.

Two partial structures of eucaryotic IMPDH enzymes from Chinese hamster (85% complete, ref *14*) and *Tritrichomonas foetus* (68% complete, ref *15*) have been reported. These structures furnished the initial information about the structure and reaction mechanism of eukaryotic IMPDH enzymes. The crystal structure of a bacterial IMPDH enzyme has not yet been reported.

To examine the differences between bacterial and mammalian IMPDH enzymes and provide a basis for the evaluation of IMPDH inhibitors as antimicrobial agents, we have expressed, characterized, and determined the crystal structure of IMPDH from a pathogenic bacterium, *Streptococcus pyogenes*. Streptococci are the most common worldwide cause of pneumonia and a leading cause of pediatric infections. Our results show that IMPDH from *S. pyogenes* has characteristics similar to other bacterial IMPDH enzymes, suggesting this enzyme will be useful in the identification of crucial residues that comprise a bacterial IMPDH enzyme signature. The high-resolution crystal structure of IMPDH from *S. pyogenes*, the first structure of a bacterial IMPDH enzyme, will provide the basis for elucidation of the distinct structural characteristics of bacterial and eukaryotic IMPDH enzymes. Knowledge of these characteristics will permit an understanding of why these enzymes exhibit functionally distinct behavior and therefore provide a foundation for the design of specific inhibitors.

MATERIALS AND METHODS

Cloning and Expression of S. pyogenes IMPDH. The coding region of IMPDH was amplified from *S. pyogenes* genomic DNA (kindly provided by Dr. Michael Boyle, Medical College of Ohio, Toledo, OH) using coding region-specific primers and a proofreading polymerase (*Pfu*). The coding sequence of *S. pyogenes* IMPDH specifies a protein of 493 amino acids that contains only a single cysteine residue at the active site (*16*). The amplified fragment was cloned into a pET23a (Novagen) expression vector and used to transform BL21(DE3)lysS bacterial cells. Sequence integrity of the expression clones was verified by DNA sequencing and analysis of the purified protein. The only notable sequence difference between the expression clones and the published sequence resulted in the substitution of a Leu in the expression clones for a Val (published sequence) at amino acid position 419. Expression of *Streptococcus* IMPDH was induced by the addition of isopropylthiogalactopyranoside (IPTG) to a concentration of 0.5 mM.

The *Streptococcus* IMPDH enzyme was purified using a modification of the procedure previously described for the human enzyme (*8*). The modified procedure replaces the Blue Sepharose dye column with a Matrex Green resin (Millipore, Bedford, MA). Since the enzyme elutes as a broad peak from the dye column, an additional chromatographic procedure was applied to facilitate enzyme concentration and increase purity. Peak fractions from the dye column are diluted with 20 mM Tris-HCl, pH 7.4, and applied to a MonoQ HR10/10 FPLC column (Pharmacia, Piscataway, NJ). The column was washed with 20 mM Tris-HCl, pH 7.4, 1 mM dithiothreitol, and the enzyme was eluted with a linear gradient of 0.2−0.7 M NaCl in wash buffer.

Purified IMPDH from *S. pyogenes* was characterized by N-terminal sequencing and analyzed by mass spectroscopy to validate as much of the internal protein sequence as possible. An N-terminal sequence was obtained (Yale Biotechnology Resource Center) for 19 residues corresponding to amino acids 2−20 of the predicted sequence and indicated cleavage of the N-terminal methionine as expected based on the presence of a serine adjacent to the N-terminal methionine (*17*). Our characterization of the purified protein also included matrix-assisted laser desorption ionization mass spectroscopy (MALDI-MS) analysis of the intact and tryptic-digested protein provided by The Biotechnology Resource Laboratory at Yale University. MALDI-MS of the intact protein indicated a molecular weight (MW) of 52 328, similar to the predicted MW of 52 657. In addition to N-terminal sequencing of the intact protein, we analyzed a tryptic digest of the purified protein by MALDI-MS. This analysis provided verification of approximately 60% of the internal protein sequence.

Selenomethionyl (SeMet) IMPDH was obtained by growth of the native expression bacterium in M9 medium. Prior to induction of IMPDH expression, de novo methionine synthesis was suppressed by the addition of phenyalanine, valine, threonine, isoleucine, leucine, and lysine to a final concentration of 50 μg/mL. Thirty minutes later, SeMet (final concentration of 50 μg/L) and IPTG (final concentration of 0.25 mM) were added. The induced bacteria were harvested 4−6 h after induction. The purification and crystallization of selenomethionyl IMPDH was as described for the wild-type enzyme, and the presence of SeMet was verified by amino acid analysis of the purified protein.

Kinetic Studies. Kinetic parameters for *S. pyogenes* IMPDH were determined by fitting initial rate data to the Michaelis−Menten equation:

$$\frac{1}{v} = \frac{1}{V_{max}} + \frac{K_m^{IMP}}{V[IMP]} + \frac{K_m^{NAD}}{V[NAD]} + \frac{K_s^{IMP} K_m^{NAD}}{V[IMP][NAD]}$$

where v is the initial rate, K_s is the dissociation constant for the enzyme/IMP complex, and K_m is the Michaelis constant. Initial velocity data were collected at varying concentrations of IMP (5−1000 μM) and NAD (50−5000 μM). The initial

Table 1: Crystal and MAD Data Collection Parameters

unit cell	$a = b = 151.49$ Å, $c = 101.67$ Å, $\alpha = \beta = \gamma = 90°$
space group	*I422*
MW (491 residues)	52657
mol/AU	1
no. of IMP	1
SeMet/AU	13

	MAD data collection (SeMet IMPDH)			
	edge (λ_2)	peak (λ_3)	remote (λ_1)	high-resolution data set
wavelength (Å)	0.9793	0.9791	1.0781	1.0332
resolution (Å)	2.5	2.5	2.5	1.90
total observations	283910	276365	272576	263355
unique reflections	20633	20627	20686	44921
redundancy	6.9	6.7	6.6	6.2
completeness	99.7	99.7	99.6	96.5
R_{merge} (%)	7.7	9.6	5.9	6.8

velocity plots followed Michaelis−Menten kinetics. Double-reciprocal plots provided a set of lines intersecting to the left of the ordinate. For IMP, the values of K_m as well as V_{max} were obtained by replotting the slopes and intercepts of these lines as a function of [NAD]. A similar strategy was employed to determine the Michaelis constant for NAD. The kinetic constants for MPA and ribavirin 5′-monophosphate (ribavirin-P) were determined by modification of Lineweaver−Burk equations for uncompetitive and competitive inhibition, respectively, in multiple substrate reactions as has been previously described (*8*).

Crystallization and Data Collection. Crystals of IMPDH from *S. pyogenes* were grown by the vapor diffusion method using hanging drops. Crystallization conditions for *S. pyogenes* human IMPDH proteins were evaluated for a variety of conditions using the Crystal Screen II kit (Hampton Research, Laguna Hills, CA). Crystals used for this study were obtained using a reservoir solution of 0.1 M MES (pH 7.2), 1.8 M ammonium sulfate, and 10 mM $CoCl_2$. Crystals were obtained by mixing various ratios of *S. pyogenes* IMPDH protein (20 mg/mL in 10 mM bis-Tris propane, pH 7.4) with reservoir solution containing 1 mM IMP and incubating at 10 °C. Over several days, the crystals grew to a maximum size of about $0.1 \times 0.1 \times 0.25$ mm^3. Crystals were transferred into a cryo-protectant solvent prepared by the addition of glycerol to the crystallization solution [final glycerol concentration (v/v), 28%] and flash-cooled in liquid nitrogen. Diffraction data were collected on beamline 19ID of the Structural Biology Center at the Advanced Photon Source (Argonne National Laboratory, Argonne, IL). The approximate X-ray flux on the sample was 4×10^{11} photons/s. Diffraction patterns from IMPDH crystals were collected at 100 K using a 3×3 mosaic CCD area detector (*18*), and all data sets were processed using the HKL2000 (*19*) package.

Crystals for the multiwavelength anomalous diffraction (MAD) study (*20*) were of SeMet IMPDH from *S. pyogenes* complexed with IMP. We recorded three data sets for a single crystal, each at a unique X-ray wavelength ($\lambda_1 = 1.0781$ Å, $\lambda_2 = 0.9793$ Å, $\lambda_3 = 0.9791$ Å, Table 1). The crystal was not oriented in any special way prior to data collection. The high-resolution data (1.90 Å) were collected from the same crystal at $\lambda = 1.0332$ Å. Details of the experiments and data quality are summarized in Table 1.

Table 2: Biochemical Comparison of *S. pyogenes* and Human Type II IMPDH

	S. pyogenes	human
molecular weight	52700	55600
active form	tetramer	tetramer
pH optimum	7.8	7.2
kinetic constants		
K_m for IMP (μM)	62 ± 19	9.2[a]
K_m for NAD (μM)	1180 ± 400	32
K_{cat} (s^{-1})	24 ± 3	1.4
inhibition characteristics (IC_{50} or K_I, nM)		
mycophenolic acid	>10000[b]	6[c]
ribavirin 5′-monophosphate	6000	390
mizoribine 5′-monophosphate	500	4
% activity with cation		
K^+	100	100
NH_4+	98	80
Rb^+	94	50
Na^+	<5	<5

[a] Reference *11*. [b] 50% inhibitory concentration (IC_{50}) at 0.5 mM IMP and 1 mM NAD. [c] K_I, reference *11*.

RESULTS

Biochemical Characteristics. S. pyogenes IMPDH monomer molecular weight is approximately 52 700 (Table 2) as determined by denaturing gel electrophoresis. Size exclusion chromatography indicates that the native form of the enzyme is a tetramer with a pH optimum of 7.8. As is observed for most IMPDH enzymes, *S. pyogenes* IMPDH has a general requirement for monovalent cations. All IMPDH enzymes thus far characterized have an active site cysteine residue that was proposed to form a covalent intermediate with IMP (*13*). The coding sequence of *S. pyogenes* IMPDH specifies a protein of 493 amino acids that contains a single cysteine residue at the active site (*16*). The essential role of this cysteine residue in *S. pyogenes* IMPDH was established by the abolition of activity observed upon treatment with 6-chloropurine, an irreversible inhibitor, or by incubation with low concentrations of iodoacetamide, a sulfhydryl reactive agent. Characterization of the kinetic parameters for this enzyme (Table 2) indicates a concurrence with other bacterial IMPDH enzymes (*9*, *10*). The bacterial enzymes effectively bind IMP but have a low affinity for NAD. Although there is considerable amino acid sequence conservation of IMPDH enzymes in the active site region (*6*), the bacterial enzymes differ from the mammalian enzymes in their affinity for NAD and in their relative sensitivity to various inhibitors (*8*−*10*). The enzyme from *S. pyogenes* has a high K_m value for NAD and is relatively insensitive to inhibition by MPA, an effective inhibitor of the mammalian enzymes. In contrast to bacterial IMPDH enzymes, enzymes from mammalian sources show distinctly lower K_m values for NAD and are effectively inhibited by MPA. These characteristics of *S. pyogenes* IMPDH suggest this enzyme is an appropriate representative of bacterial IMPDH and can be used to examine the differences between the bacterial and eukaryotic forms of IMPDH.

Structure Determination. To investigate the basis for the different characteristics of bacterial and mammalian IMPDH, we determined the crystal structure of *S. pyogenes* IMPDH at 1.9 Å resolution by replacing all methionine residues in the enzyme with selenomethionine and applying MAD phasing methods (*20*). Phase analysis was initiated by

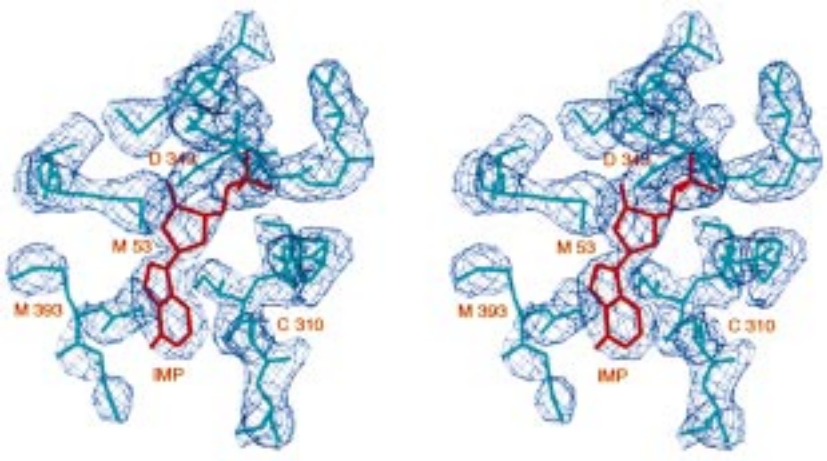

FIGURE 2: Stereoview of the electron density map around the active site. Solvent-flattened MAD map calculated at 2.5 Å resolution drawn at a contour level of 1.2 σ.

molecular replacement using AMORE (*21*) and the *T. foetus* atomic coordinates (*15*) from the PDB as a search model. IMPDH from *T. foetus*, a eucaryotic organism, shows poor homology to *S. pyogenes* IMPDH (35% identity). As a consequence of the poor homology and the incompleteness of the *T. foetus* IMPDH structure, the initial molecular replacement solution produced phases that were not sufficiently close to the correct values for the structure to be interpreted further. However, this phase set was sufficiently good to identify 6 of the 13 selenium sites in the structure. Refinement using MLPHARE (*22*) permitted identification of all remaining selenium atoms. Successive refinement cycles produced a map from which we could complete the interpretation of the model (Figure 2). Phases were improved during subsequent refinement with CNS (*23*) (see below), permitting modeling of 97% of the structure.

Model Building and Refinement. All model building was carried out with FRODO (*24*) on an Evans and Sutherland ESV10 graphics workstation. Refinement of the initial model against the MAD data was carried out using torsion-angle molecular dynamics (*25*) and the phase-restrained MLHL target (*26*) implemented in CNS (*23*). Diffraction data from 6 to 1.90 Å were used throughout the refinement except for a 4% randomly selected test set required for cross-validation of the σ_A values used in the maximum-likelihood target and R_{free} calculations. A flat bulk solvent model (*27*) was implemented in density modification of the initial MAD maps, with the program DM (*27*). At the later stages, σ_A phase-combined maps (*22*) were calculated, with model phases calculated from the MLHL refined model combined with experimental phases. Alternate cycles of model rebuilding, positional refinement, restrained *B*-factor refinement, and water placement followed, decreasing the free *R*-factor from its initial value of 48% to 25.8% and yielding a final *R*-factor of 23.4%. Solvent molecules were identified using several cycles of WATERPICK program within the CNS package. We located 422 solvent molecules per monomer. The average *B*-factors for protein atoms, catalytic domain, CBS domain, and solvent atoms are listed in Table 3; the *B*-factor for solvent atoms ranged from 20 to 69 Å^2. The model has a correlation coefficient (F_o versus F_c) of 95% and an estimated coordinate error of 0.3 Å from SIGMAA (*28*). Stereochemical and other refinement parameters are given in Table 3. By PROCHECK (*29*) criteria, the model has 91.2% of the main chain torsion angles within the "allowed regions" of the Ramachandran plot and 8.8% within the "additional allowed regions". There are no residues in "disallowed regions".

Table 3: Crystallographic Statistics

	Phasing							
	acentric			centric			all	
resolution (Å)	no.	fom[a]	phasing[b] power	no.	fom	phasing power	no.	fom
7.3−2.5	18189	0.64	2.02	1873	0.60	1.63	20062	0.64

Refinement Statistics	
resolution range (Å)	6.0−1.90
reflections	40828
σ cutoff	none
R-value[c] (%)	23.4
free *R*-value[d] (%)	25.8 (1690 reflections)
completeness (%)	88.6
no. of non-hydrogen atoms	3997
no. of solvent molecules	422
no. of IMP	1
bond length deviation (Å)	0.0059
bond angle deviation (deg)	1.3029
improper angle deviation (deg)	0.745
dihedrals deviation (deg)	21.702
average B-factor (Å^2)	
protein atoms	37.5
catalytic domain	34.4
CBS dimer domain	43.4
solvent atoms	50.1
residues in core phi-psi regions (%)	91.2
residues in disallowed regions (%)	0.0

[a] Figure of merit is a measure of the relative reliability of a phase based on the consistency of the MIR analysis from one derivative to the next. The maximum value is 1.0. [b] MAD phasing power is defined: $\{\langle|F_{h1} - F_{hi}|\rangle/\int_\phi P_{\lambda 1\rightarrow\lambda i}(\phi)(||F_{\lambda 1}|e^{i\phi} + F_{hi} - F_{h1}| - |F_{\lambda i}|)^2\, d\phi\}^{1/2}$, computed for individual lack-of-closure expressions between the reflections of the reference wavelength λ_1, its Friedel mate, and the Bijvoet pairs measured at the other wavelengths (F_{hi}). $P_{\lambda 1\rightarrow\lambda i}(\phi)$ is the corresponding phase probability distribution. [c] *R*-value $= (|F_{obs}| - \kappa|F_{calc}|)/|F_{obs}|$. [d] Free *R*-value is the *R*-value obtained for a test set of reflections (4% of the diffraction data) not used during refinement or σ_A calculations.

Tetramer Organization. S. pyogenes IMPDH is a tetramer with its four subunits related by a crystallographic 4-fold axis. Each monomer has a two-domain structure (Figure 3A): a catalytic domain (40 × 40 × 50 Å^3, amino acid residues 2−92 and 224−492) forming the interior core of the active tetrameric enzyme and a CBS dimer domain (20

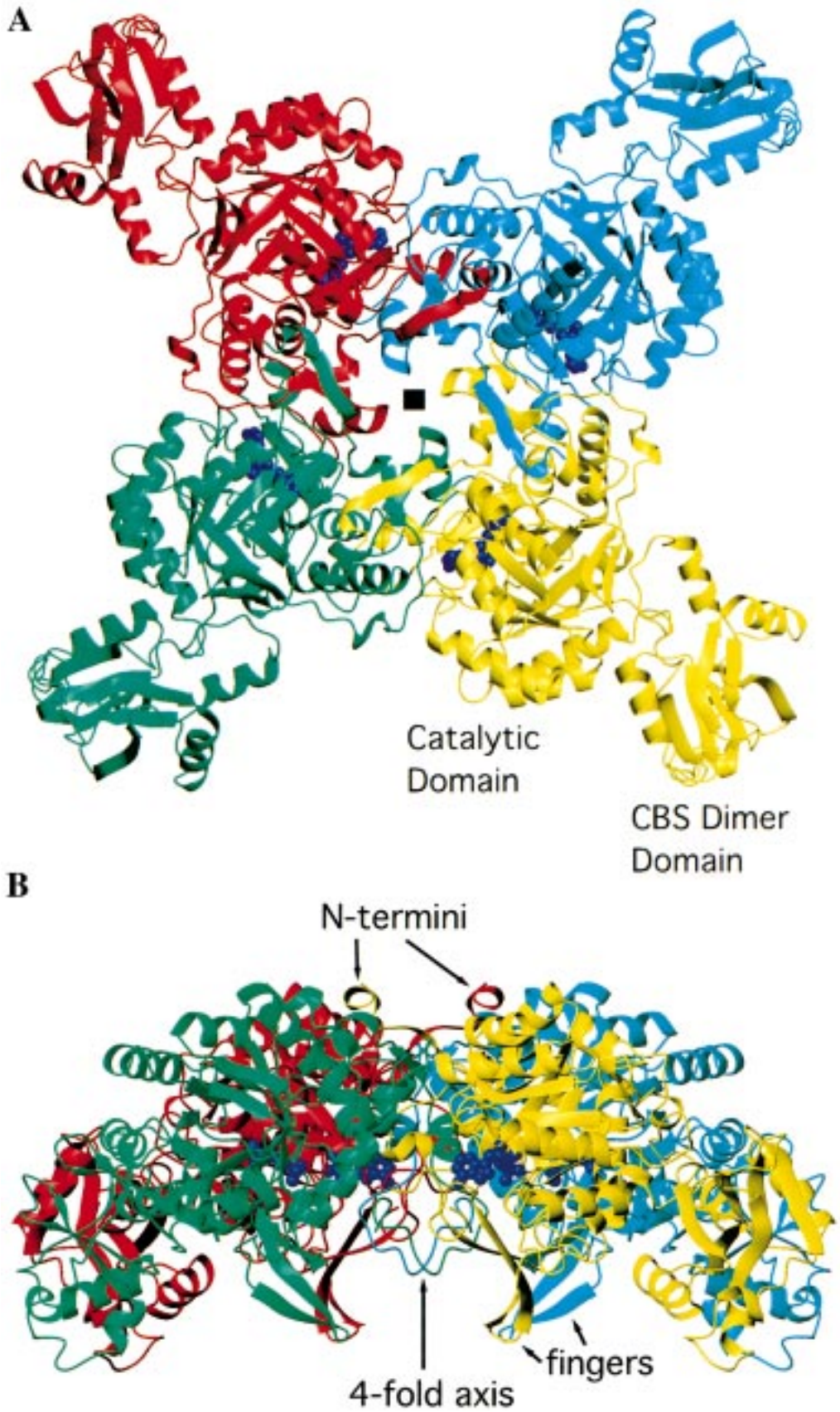

FIGURE 3: Ribbon drawing of the catalytically active IMPDH tetramer. The tetramer is displayed (A) parallel and (B) perpendicular to the 4-fold axis. Each subunit is shown in a different color with a space-filling model of IMP in the active site of each subunit.

$\times$ 20 $\times$ 30 Å^3, residues 93−223) projecting outward from the corners of the square. The CBS designation arises from the original identification of this folding motif in the enzyme cystathionine β-synthase. The catalytic domain contains the active site positioned near the tetramer 4-fold at the subunit interface (Figure 3B).

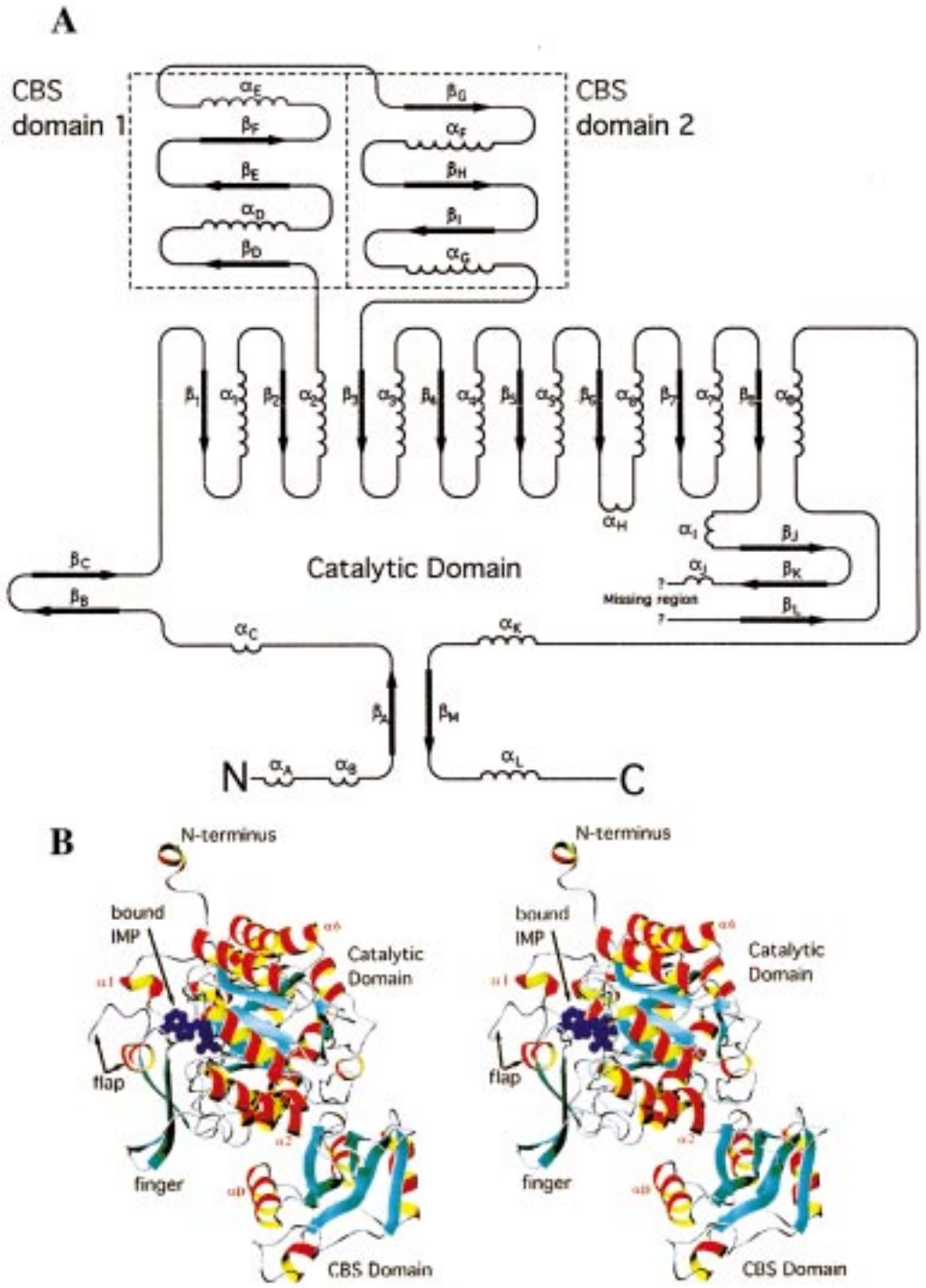

FIGURE 4: Secondary structure of the IMPDH monomer. (A) Topology diagram of IMPDH domains. Secondary structure was assigned using the Kabsch and Sander (39) algorithm along with visual inspection. The α-helices and β-strands that form the TIM barrel core are labeled α1−α8 and β1−β8. The remaining strands and helices are designated in alphanumeric order (e.g., αA−αL). The part of the structure not visible in the electron density maps is marked as "????". (B) Stereoview ribbon diagram arranged approximately perpendicular to the axis of the TIM barrel. The secondary structure elements are shown as red/yellow α-helices and blue β-strands. IMP is shown as a blue ball-and-stick model.

A feature observed in the tetrameric structure is an extended region projecting from the C-terminal face of each monomeric subunit (Figure 3B). These finger structures are composed of two antiparallel β-strand structures (β_J, β_K; Figure 4A) stabilized by hydrogen bonding and interactions with the β_L region. The finger region is not involved in catalysis but is found in all IMPDH enzymes.

Catalytic Domain. The core of the catalytic domain (Figure 4B) is a TIM barrel providing a scaffold for the attachment of additional structural and catalytic moieties. This core contains eight parallel α/β motifs with the active site near the C-terminus of the β-strands. Sequence comparisons suggest limited sequence conservation within the TIM barrel core relative to the high level of conservation observed for residues forming the catalytic site pocket (*6*). The sequence conservation of the TIM barrel is restricted to residues adjacent to the active site pocket and to a region representing the junction between the catalytic and CBS dimer domains.

There are several large structural and catalytic protrusions from the TIM barrel surface. The N-terminus protrudes from strand β_1 on the distal face of the TIM barrel (furthest from the IMP binding pocket). The CBS dimer domain is located between helix α_2 and strand β_3. Connections between the remaining α/β motifs are short (2−5 amino acid residues) and contain many proline, glycine, and hydrophobic residues. The C-terminal region exits from helix α_8, on the opposite face of the tetramer from the N-terminus.

The protrusions on the proximal face of the TIM barrel scaffold range in size from 3 to 67 residues and define the character of the active site. Three of the barrel connections (β_1/α_1, β_6/α_6, and β_7/α_7) show greater than a 50% amino acid sequence conservation for all IMPDH proteins. The β_8/α_8 protrusion is the largest (67 residues) of the proximal face motifs and contains the "finger" structure (Figure 3B), short helices α_I and α_J, strands β_{J-L}, and regions that have a role in catalysis and that interact with other IMPDH monomers in the tetramer. This protrusion sequence is also highly conserved, with regional sequence conservation of 60−80% in 3 distinct 10-amino acid-residue segments. A distinct feature of this region is a "flap" (residues 396−419) on one edge of the active site that shows very poor electron density and apparently projects into the solvent (Figure 4B). In the *S. pyogenes* IMPDH 1.9 Å structure, 14 residues in this flap are disordered in the presence of substrate in the active site. In crystals of eucaryotic IMPDH containing product and transition-state analogue and complexed with MPA (*14*, *15*), this region is also disordered. It has been suggested (*15*) that this flap functions by folding over the catalytic pocket, controlling access to and ordering the active site, perhaps in a manner similar to the active site flap of lactate dehydrogenase (*30*).

CBS Dimer Domain. The CBS dimer domain, found in IMPDH proteins from all three kingdoms, is composed of two CBS motifs (Figure 4A,B) related by approximate 2-fold symmetry (rms deviations between related C_α atoms: 2.7 Å). Each CBS motif has the characteristic sheet/helix/sheet/sheet/helix topology. This is the first reported complete structure of a CBS dimer domain: a folding motif originally identified in cystathionine β-synthase and proposed to act as a regulatory element since mutations lead to the human disease homocystinuria (*31*). The CBS dimer domain in IMPDH does not interact with the other subunits in the active tetrameric enzyme and may not be required for activity (*9*, *14*). In *S. pyogenes* IMPDH, two CBS domains form a minibarrel structure that has a distinct hydrophobic core. Among bacteria, the degree of amino acid conservation is highest in the E/F and H/I β-strands (Figure 4A,B) that span the interior of the CBS dimer domain and provide a resource of hydrophobic residues. The α-helices on the exterior maintain the character of this domain with hydrophilic residues on the exterior surfaces and hydrophobic residues positioned on the interior. There is a well-defined cleft between CBS motifs (approximately 15 Å in length) that may function as a potential binding site for regulatory molecules. There is no known role for CBS motifs in bacteria, but in eukaryotic organisms they appear to mediate cytoplasmic targeting, protein−protein interactions, or protein regulation (*31*).

Catalytic Site and Implication for the Mechanism of Bacterial IMPDH. A unique aspect of the *S. pyogenes* IMPDH structure is that it allows examination of the initial stage of the catalytic cycle. IMP is bound at one end of the TIM barrel, with the other end blocked by the β_B/β_C sheet (Figure 4A,B). Short helices H, J, and I are structural motifs containing many of the active site residues. During the reaction, a hydride is transferred from the C2 carbon of the hypoxanthine ring to NAD, and an oxygen atom is substituted in the C2 position, resulting in the formation of xanthine.

The high-resolution (1.9 Å) crystal structure of *S. pyogenes* IMP dehydrogenase allows examination of the catalytic site in greater detail than was previously possible. The are a number of protein interactions with the IMP ribose and phosphate moieties (Figure 5A). The ribose is in the C2′-*endo*-conformation. Its 2′- and 3′-hydroxyls are hydrogen-bonded with Asp343 and a water molecule that, through a water relay system, connects with N3 of the hypoxanthine ring. The phosphate group is anchored in its site by a number of amino acid side chains (Ser308, Ser367, and Tyr 390) and three main chain nitrogen atoms (Gly345, Gly366, and Ser367). Ile309 stacks on top of the hypoxanthine ring, and four hydrogen bonds further stabilize the ring (Figure 5A).

Cysteine 310 has been identified previously as a key residue in catalysis (*12*, *13*). The ability of the thiol residue to ionize appears to be critical for the reaction involving nucleophilic attack. The hydroxyl of Thr312 is in position (3.3 Å) to activate Cys310 (Figure 5B). Covalent bond formation requires reorientation of the hypoxanthine ring (rotation around the glycosidic bond) and nucleophilic attack on C2 by Cys310. This mechanism is consistent with the proposed formation of a tetrahedral intermediate (*32*). However, our data show that IMPDH does not form a covalent bond with the substrate in the absence of the NAD cofactor. This suggests that NAD may have multiple roles as hydride acceptor and substrate activator, as well as in contributing to the structure of the active site pocket.

The hamster IMPDH structure (*14*) contains the hypoxanthine ring covalently bound to the active site cysteine and the inhibitor MPA bound in the active site. It appears that the hamster IMPDH structure represents the covalent thioimidate intermediate of the reaction in which MPA, an uncompetitive inhibitor, prevents the hydrolysis of the thiopurine covalent intermediate, as suggested by Link and Straub (*33*). It has been suggested that MPA restricts the access of the solvent molecules and blocks subsequent steps of the reaction (*14*). This observation also suggests that the hydrolysis of the thioimidate intermediate is mediated by an activated water molecule originating from the NAD site. In the *S. pyogenes* IMPDH structure, we have located two water residues that are potential candidates for nucleophilic attack on the thioimidate (Figure 5B), and several residues (Glu421, Thr312, and Tyr450′) can act as activators of a water molecule. However, since the enzyme does not contain NAD, a required cofactor, elucidation of the mechanistic details of the hydrolysis reaction will require additional studies. Because MPA can stabilize the thioimidate intermediate in the human enzyme (*14*), hydrolysis of thioimidate must be several orders of magnitude slower than the dissociation of NADH, a result consistent with the mechanism proposed by Wang et al. (*11*).

Site-Specific Mutants. To validate the role of specific residues in catalysis and to provide a basis for comparing the bacterial and mammalian enzymes, we constructed several point mutants. The sites for mutation were selected on the

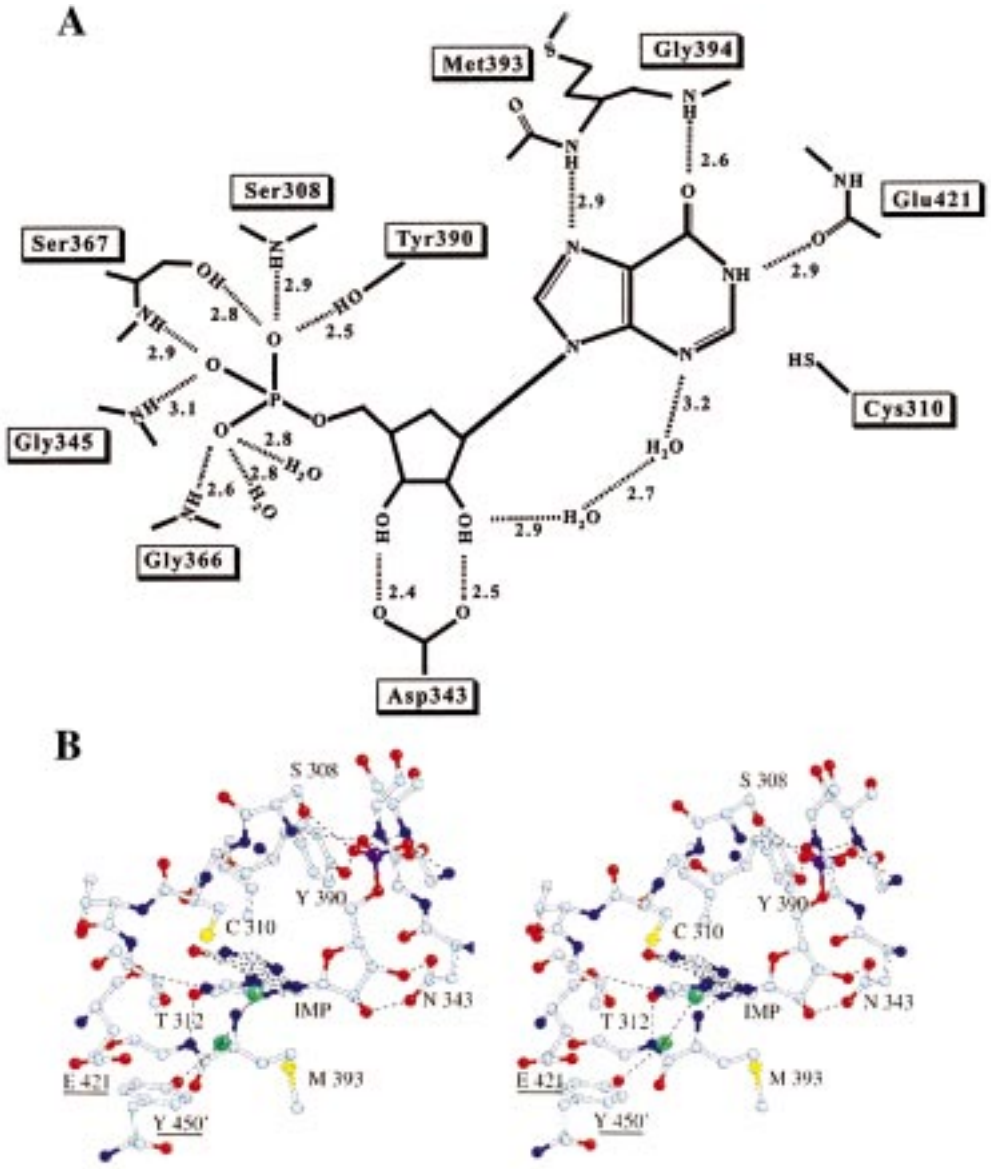

FIGURE 5: IMPDH active site. (A) Cartoon of bound IMP showing side chain interactions and active site residues. Water molecules are colored green. (B) Stereoview ball-and-stick diagram of bound IMP illustrating the alignment of the hypoxanthine ring relative to the catalytic Cys310 residue. The dashed ring cartoon indicates the proposed realignment of the hypoxanthine ring initiated by NAD binding. Residues targeted for mutagenesis (E421 and Tyr450′) are underlined. The "′" symbol on T450 indicates a symmetry-related molecule.

Table 4: Site-Specific Mutants of *S. pyogenes* Impdh

mutant	corresponding residue in mammalian IMPDH	region		relative specific activity of purified protein
		location	function	
Arg406→Ala	Arg	active site flap	catalysis	no activity
Tyr450→Asp	Asp	helix 8, TIM barrel	unknown	no activity
Tyr450→Ala	Asp	active site	unknown	0.25
Glu421→Gln	Gln	α_J/β_L loop	NAD binding region	1.0

basis of previous studies suggesting a catalytic role for the region and supported by information derived from the *S. pyogenes* IMPDH crystal structure. One region targeted for site-specific mutagenesis was the active site flap. This flap is present in all IMPDH enzymes and is disordered in the *S. pyogenes* IMPDH structures and in the IMPDH structures from hamster and *T. foetus*. Although this region has not been previously implicated in the catalysis mechanism of IMPDH enzymes, the presence of a conserved RY(FY) motif and the similarities to the flap region in lactate dehydrogenase (*30*) suggest a potential role in catalysis. Mutation of Arg406 to alanine in this flap region results in a complete loss of enzyme activity (Table 4) as might be expected for a residue conserved in all IMPDH enzymes. This loss of activity confirms the importance of the active site flap in catalysis. Since there is little sequence conservation of this region, this structure is an attractive target for specific inhibitors.

The catalytic mechanism of *S. pyogenes* IMPDH involves the hydrolysis of a thioimidate intermediate that we believe is mediated by an activated water molecule originating from

the NAD site. In the *S. pyogenes* IMPDH structure, we have located two water residues that are potential candidates for nucleophilic attack on the thioimidate. Tyr450′, originating from an adjacent subunit, is a residue in the active site pocket that can act as an activator of one of these water molecules. This residue is located at the noncatalytic end of a conserved helix (helix 8) that forms the TIM barrel core. Replacement of Tyr450 with aspartic acid or alanine (Table 4) results in substantial loss of enzyme activity. Approximately 25% activity is retained for an alanine replacement, but substitution of aspartic acid results in a loss of enzyme activity. This region is conserved in the IMPDH enzymes, but the sequence pattern is different in bacteria and eukaryotes, suggesting this region may contribute to the differential signature of the bacterial and mammalian enzymes.

The NAD binding region (between the α_J/β_L loop) was also selected as a target for site-specific mutagenesis. The selection of Glu421 for mutation was based on an analysis of sequence differences at residues corresponding to or near amino acids identified as MPA binding sites in human IMPDH. The conserved glutamate in bacteria is replaced with a conserved glutamine in eukaryotes. This substitution does not alter the apparent activity of *S. pyogenes* IMPDH (Table 4). This result was unexpected since replacement of the corresponding residue in the hamster enzyme (Gln441) with alanine results in a significant decrease in activity (*14*).

DISCUSSION

Because of its central role in purine metabolism, IMPDH is an attractive therapeutic target. Several recent reviews have outlined the utility of mammalian IMPDH inhibitors as anticancer (*34*) or antiviral (*35*) agents or as immunosuppressive drugs (*36*). Although there are no selective inhibitors of bacterial IMPDH enzymes, such compounds could have potential application as antimicrobial agents. This proposal is supported by the observation that bacterial and mammalian IMPDH enzymes provide the same catalytic function but have a set of unique structural and biochemical characteristics. The kinetic and biochemical characteristics of *S. pyogenes* IMP dehydrogenase are similar to other bacterial IMPDH enzymes but different from mammalian IMPDH enzymes. Relative to the mammalian enzymes, the bacterial enzymes bind NAD poorly and are inhibited by MPA only at very high concentrations (Table 2). Elucidation of the basis of these distinct characteristics will aid the design of specific IMPDH inhibitors.

The structure of *S. pyogenes* IMPDH provides a new resource to define the distinct characteristics of bacterial and mammalian IMPDH enzymes. Features such as the catalytic pocket loops, active site flap region, and CBS dimer domain are structurally conserved but show a different pattern of sequence conservation in bacteria and eukaryotes, suggesting that they could contribute to the differential signature of the bacterial and mammalian enzymes. Analysis of sequence alignments for this region indicates a pattern of catalytic residues conserved in all enzymes and a secondary pattern of amino acid conservation associated with either bacterial or eukaryotic IMPDH enzymes. This observation is supported by our site-specific mutants at positions Glu421 and Tyr450 that appear to differentially alter the activity of the mammalian and bacterial IMPDH enzymes. Residue Tyr450 in *S. pyogenes* IMPDH is located at the noncatalytic end of the TIM barrel. However, this region has contacts with another molecule in the tetramer and contributes to the catalytic environment of the adjacent monomer (Figure 5B). Our site-specific mutagenesis results show partial retention of activity with an alanine substitution but no activity with an aspartic acid substitution for this residue. Aspartic acid was selected as a replacement on the basis of sequence alignments that show 12 of 13 eucaryotic enzymes contain aspartic acid at the corresponding position (the exception being asparagine in *T. foetus*). The partial activity observed with the Ala replacement suggests Tyr450 does not have an essential role in catalysis but does contribute to the environment of the catalytic pocket. Further analysis of this region will provide insight into the differences in the environment of the catalytic pocket in bacterial and eucaryotic enzymes and also the role of the tetrameric form of the active enzyme.

The Glu421 in *S. pyogenes* IMPDH is conserved in bacteria while eucaryotic IMPDH enzymes contain glutamine in the corresponding position. In hamster IMPDH, the corresponding residue, Gln441, is implicated in the binding of MPA. Comparison of the residues involved in MPA binding in the hamster enzyme (Asp274, Ser276, Asn303, Arg322, Gly326, Thr333, Gln441) with the equivalent residues in *S. pyogenes* IMPDH indicates that these residues are largely conserved. The aspartic acid, asparagine, glycine, and threonine residues are identical, but threonine replaces Ser276 (although serine is present in other bacterial enzymes), and Lys301 replaces the hamster Arg322 residue. The most significant change appears to be replacement of Glu421 with Gln441 (interestingly, this residue is part of the active site flap). Although this suggests that the NAD binding pockets of hamster and bacterial IMPDH differ, we did not observe a change in activity upon substitution of glutamine for glutamic acid at position 421. It is possible that this substitution does not affect the observed activity but may alter the sensitivity to MPA. Further studies are in progress to define the contribution of the sequence signature in this region to the bacterial kinetic profile.

The active site flap represents another region that could account for the kinetic and biochemical differences between IMPDH enzymes. This flap is present in all IMPDH enzymes and is disordered in the IMPDH structures from hamster, *T. foetus*, and *S. pyogenes*. This persistent disorder suggests that NAD binding is essential for structuring the flap, a suggestion supported by the resistance of this region to proteolysis acquired by NAD binding (*37*). This also implies that MPA binding does not involve an interaction with this flap and does not entirely mimic NAD binding. This flap may therefore be important in mediating NAD binding specificity in the active site and may be responsible for some of the kinetic differences observed between IMPDH enzymes from bacteria and eukaryotes. Sequence comparisons indicate that loop size is conserved but sequence conservation is limited. A conserved feature of this region is the presence of arginine adjacent to one or two aromatic residues. Since IMP and NAD bind sequentially to the active site, these residues may bind to the NAD moiety, thereby ordering the active site. Our preliminary site-specific mutagenesis results implicate this region as essential for enzyme activity, but further studies will be necessary to define the specific role of the flap region. The sequence heterogeneity observed in this flap region may

also account for the discriminatory features of bacterial and mammalian IMPDH enzymes.

The finger region and the CBS dimer domain are not involved in catalysis but are found in all IMPDH enzymes. These regions show little sequence conservation but have been structurally conserved. The finger structure is composed of two antiparallel β-strand structures stabilized by hydrogen bonding and interactions with the βL region. The CBS dimer domain contains two CBS motifs arranged on a pseudodyad axis. In other proteins (e.g., cystathionine β-synthase and chloride channel proteins), mutations in these domains are associated with pathologic consequences. It has also been suggested (*31*) that these domains may be involved in cytoplasmic targeting or other regulatory functions. In either case, the metabolic expenditure required for conservation of these structures suggests an underlying functional role.

A unique aspect of the *S. pyogenes* IMPDH structure is that it allows examination of the initial stage of the catalytic cycle. Our data show IMP does not form a covalent bond in the absence of NAD. Covalent bond formation requires reorientation of the hypoxanthine ring and nucleophilic attack on C2 by Cys310. We propose that NAD binding initiates realignment of the hypoxanthine ring and facilitates the electron shift with the ring required for formation of the thioimidate intermediate. This suggests that NAD may have multiple roles as hydride acceptor, substrate activator, and also in contributing to the structure of the active site pocket.

The structure of *S. pyogenes* IMPDH allows for a detailed comparison of the eukaryotic and bacterial enzymes. It will also provide the basis for an explanation for the unique properties of the bacterial enzymes. In conjunction with additional site specific mutants and kinetic analyses, the characteristics and structure of *S. pyogenes* IMPDH will be useful in the delineation of specific characteristics of bacterial and mammalian IMPDH enzymes. This knowledge will contribute to the design of inhibitors that specifically target bacterial IMPDH enzymes.

ACKNOWLEDGMENT

This work and the use of the Structural Biology Center beamline at Argonne National Laboratory's Advanced Photon Source were supported by the U.S. Department of Energy, Office of Biological and Environmental Research, under Contract W-31-109-ENG-38. We acknowledge the contributions of the Structural Biology Center staff, especially Gerd Rosenbaum and Randy Alkire. We thank Axel Brünger and Paul Adams of Yale University for helpful discussions and use of the CNS package prior to official release. We express our thanks to Wladek Minor and Zbyszek Otwinowski for use of the HKL2000 package prior to official release and to Marianne Schiffer, Fred Stevens, Phani Pokkuluri, and Martin Walsh for their helpful suggestions and critical review of the manuscript.

REFERENCES

1. Collart, F. R., and Huberman, E. (1990) *Blood 75*, 570−576.
2. Kiguchi, K., Collart, F. R., Henning-Chubb, C., and Huberman, E. (1990) *Cell Growth Differ. 1*, 259−270.
3. Smith, D. W., Frankel, L. R., Mathers, L. H., Tang, A. T., Atiagno, R. L., and Prober, C. G. (1991) *N. Engl. J. Med. 325*, 24−29.
4. Jayaram, H. N., Gearehbaghi, K., Jayaram, N. H., Rieser, J., Krohn, K., and Paull, K. D. (1992) *Int. J. Cancer 51*, 182−188.
5. Allison, A. C., and Eugui, E. M. (1996) *Clin. Transplant. 10*, 77−84.
6. Collart, F. R., Osipiuk, J., Trent, J., Olsen, G. J., and Huberman, E. (1996) *Gene 174*, 206−216.
7. Collart, F. R., Osipiuk, J., Trent, J., Olsen, G. J., and Huberman, E. (1996) *Gene 174*, 217−220.
8. Hager, P. W., Collart, F. R., Huberman, E., and Mitchell, B. S. (1995) *Biochem. Pharmacol. 49*, 1323−1329.
9. Zhou, X., Cahoon, M., Rosa, P., and Hedstrom, L. (1997) *J. Biol. Chem. 272*, 21977−21981.
10. Kerr, K. M., and Hedstrom, L. (1997) *Biochemistry 36*, 13365−13373.
11. Wang, W., Papov, V. V., Minakawa, N., Matsuda, A., Biemann, and Hedstrom, L. (1996) *Biochemistry 35*, 95−101.
12. Huete-Pérez, J. A., Wu, J. C., Whitby, F. G., and Wang, C. C. (1995) *Biochemistry 34*, 13889−13894.
13. Antonino, L. C., Straub, K., and Wu, J. C. (1994) *Biochemistry 33*, 1760−1765.
14. Sintchak, M. D., Fleming, M. A., Futer, O., Raybuck, S. A., Chambers, S. P., Caron, P. R., Murcko, M. A., and Wilson, K. P. (1996) *Cell 85*, 921−930.
15. Whitby, F. G., Luecke, H., Khun, P., Somoza, J. R., Huete-Perez, J. A., Phillips, J. D., Hill, C. P., Fletterick, R. J., and Wang, C. C. (1997) *Biochemistry 36*, 10666−10674.
16. Ashbaugh, C. D., and Wessels, M. R. (1995) *Gene 165*, 57−60.
17. Hirel, Ph.-H., Schmitter, J.-M., Dessen, P., Fayat, G., and Blanquet, S. (1989) *Proc. Natl. Acad. Sci. U.S.A. 86*, 8247−8251.
18. Westbrook, E. M., and Naday, I. (1997) *Methods Enzymol. 276*, 244−268.
19. Otwinowski, Z., and Minor, W. (1997) *Methods Enzymol. 276*, 307−326.
20. Hendrickson, W. A. (1991) *Science 254*, 51−58.
21. Navaza, J., and Sludijan, P. (1997) *Methods Enzymol. 276*, 581−594.
22. Otwinowski, Z. (1991) in *Isomorphous Replacement and Anomalous Scattering* (Wolf, W., Evans, P. R., and Leslie, A. G. W., Eds.) pp 80−86, Science and Engineering Research Council, Daresbury, England.
23. Brünger, A. T., Adams, P. D., Clore, G. M., DeLano, W. L., Gros, P., Grosse-Kunstleve, R. W., Jiang, J. S., Kaszenski, J., Nigles, M., Pannu, N. S., Read, R. J., Rice, L. M., Simonson, T., and Warren, G. L. (1998) *Acta Crystallogr., Sect. D 54* (Part 5), 905−921.
24. Jones, T. A. (1985) *Methods Enzymol. 151*, 157−171.
25. Rice, L. M., and Brünger, A. T. (1994) *Proteins: Struct., Funct., Genet. 19*, 277−290.
26. Pannu, N. S., Murshudov, G. N., Dodson, E. J., and Read, R. (1998) *Acta Crystallogr., Sect.* D (in press).
27. Cowtan, K. D. (1994) *Jt. CCP4 ESF−EACBM Newsl. Protein Crystallogr. 31*, 34−38.
28. Read, R. J. (1986) *Acta Crystallogr., Sect. A42*, 140−149.
29. Laskowski, R. A., Macarthur, M. W., Moss, D. S., and Thornton, J. M. (1993) *J. Appl. Crystallogr. 26*, 283−291.
30. Holbrook, J., Liljas, A., Steindel, S. J., and Rossman, M. G. (1975) in *The Enzymes* (Boyer, P. D., Ed.) pp 191−203, Academic Press, New York.
31. Bateman, A. (1997) *Trends Biochem. Sci. 22*, 12−13.
32. Xiang, B., and Markham, G. D. (1997) *Arch. Biochem. Biophys. 388*, 378−382.
33. Link, J. O., and Straub, K. (1996) *J. Am. Chem. Soc.* 118, 2091−2092.
34. Pankiewicz, K. W. (1997) *Pharmacol. Ther. 76*, 89−100.
35. Andrei, G., and De Clercq, E. (1993) *Antiviral Res. 22*, 45−75.
36. Halloran, P. F. (1996) *Clin. Transplant. 10*, 118−123.
37. Nimmesgern, E., Fox, T., Fleming, M. A., and Thomson, J. A. (1996) *J. Biol. Chem. 271*, 9421−19427.
38. Kabsch, W., and Saunder, C. (1983) *Biopolymers 22*, 2577−2637.

BI982858V